Virologica Sinica (2019) 34:397–411
https://doi.org/10.1007/s12250-019-00120-5

www.virosin.org
www.springer.com/12250

RESEARCH ARTICLE

Mitochondria Redistribution in Enterovirus A71 Infected Cells and Its Effect on Virus Replication

Yang Yang[1,2] · Haolong Cong[1] · Ning Du[3] · Xiaodong Han[4] · Lei Song[1] · Wenliang Zhang[1] · Chunrui Li[1,2] · Po Tien[1,2]

Received: 21 December 2018 / Accepted: 25 March 2019 / Published online: 8 May 2019
© Wuhan Institute of Virology, CAS 2019

Abstract

Enterovirus A71 (EV-A71) is one of the main causative agents of hand, foot and mouth disease (HFMD) and it also causes severe neurologic complications in infected children. The interactions between some viruses and the host mitochondria are crucial for virus replication and pathogenicity. In this study, it was observed that EV-A71 infection resulted in a perinuclear redistribution of the mitochondria. The mitochondria rearrangement was found to require the microtubule network, the dynein complex and a low cytosolic calcium concentration. Subsequently, the EV-A71 non-structural protein 2BC was identified as the viral protein capable of inducing mitochondria clustering. The protein was found localized on mitochondria and interacted with the mitochondrial Rho GTPase 1 (RHOT1) that is a key protein required for attachment between the mitochondria and the motor proteins, which are responsible for the control of mitochondria movement. Additionally, suppressing mitochondria clustering by treating cells with nocodazole, EHNA, thapsigargin or A23187 consistently inhibited EV-A71 replication, indicating that mitochondria recruitment played a crucial role in the EV-A71 life cycle. This study identified a novel function of the EV-A71 2BC protein and provided a potential model for the regulation of mitochondrial motility in EV-A71 infection.

Keywords Enterovirus A71 (EV-A71) · Mitochondria · Microtubule network · Calcium concentration · Mitochondrial Rho GTPase 1 (RHOT1)

Introduction

Enterovirus A71 (EV-A71) is a positive-strand RNA virus which belongs to the *Enterovirus* genus of the *Picornaviridae* family. It was first isolated from the feces of an infant suffering from encephalitis and identified in 1969 in California, USA (Schmidt *et al.* 1974). Its genome contains approximately 7.4 kilobases RNA and encodes a single polyprotein that is processed into 4 structural proteins (VP1, VP2, VP3 and VP4) and 7 non-structural proteins (2A, 2B, 2C, 3A, 3B, 3C and 3D). Besides, several precursor proteins such as 2BC, 3AB and 3CD were reported to have specific functions in virus replication (Weidman *et al.* 2003; Tang *et al.* 2014; Lai *et al.* 2017).

EV-A71 is one of the main causative agents of hand, foot and mouth disease (HFMD), and it may also cause severe neurologic complications such as aseptic meningitis, brainstem encephalitis, flaccid paralysis and neurogenic pulmonary edema, leading to high fatality rates in children (Huang *et al.* 1999; Solomon *et al.* 2010). In the past

Electronic supplementary material The online version of this article (https://doi.org/10.1007/s12250-019-00120-5) contains supplementary material, which is available to authorized users.

Yang Yang and Haolong Cong have contributed equally to this study.

✉ Po Tien
tienpo@sun.im.ac.cn

1 Center for Molecular Virology, CAS Key Laboratory of Pathogenic Microbiology and Immunology, Institute of Microbiology, Chinese Academy of Sciences, Beijing 100101, China

2 University of the Chinese Academy of Sciences, Beijing 100101, China

3 Beijing Institutes of Life Science, Chinese Academy of Sciences, Beijing 100101, China

4 College of Life Sciences, Inner Mongolia Agriculture University, Hohhot 010018, China

decades, EV-A71 outbreaks have occurred worldwide with increasing frequency and scale, especially in the Asia–Pacific region (Solomon *et al.* 2010). Although inactivated EV-A71 vaccines have been available recently (Yi *et al.* 2017), no specific therapy has been developed to treat this viral disease, partly due to a lack of understanding of the mechanisms involved in EV-A71 infection.

Mitochondria are multifunctional eukaryotic organelles with diverse roles, including energy production and distribution, apoptosis, innate immunity, metabolic regulation, cell-cycle control and signal transduction (Gogvadze and Orrenius 2006; McBride *et al.* 2006; Seth *et al.* 2006). This makes them a target for various kinds of viruses, such as human immunodeficiency virus (HIV), hepatitis C virus (HCV) and influenza A virus (Arunagiri *et al.* 1997; Danishuddin *et al.* 2010; Wang and Weinman 2013). EV-A71 has been reported to inhibit type I interferon response and impact mitochondrial apoptotic pathway by targeting host mitochondria (Wang *et al.* 2013; Cong *et al.* 2016). It also induces mitochondria generation of reactive oxygen species (ROS) to facilitate its replication (Cheng *et al.* 2014). In a previous report, we described perinuclear migration of mitochondria in EV-A71-infected cells and regarded it as the recruitment of mitochondria to the virus replication center (Cong *et al.* 2013). However, the molecular mechanism of mitochondria redistribution and its influence on EV-A71 replication remained elusive.

In the present study, we revealed the EV-A71-induced mitochondria redistribution and identified the cellular and viral factors involved in this process. Our results provided an insight into the mechanism of mitochondria recruitment during EV-A71 infection which was suggested to be an essential process in the EV-A71 life cycle.

Materials and Methods

Cell Culture, Virus Strains and Virus Infection

The enterovirus A71 (EV-A71) strain Hubei-09 was kindly provided by Prof. Bo Zhang at Wuhan Institute of Virology, Chinese Academy of Sciences, Wuhan, China. Human cervical (HeLa) cells were propagated and maintained in Double Modified Eagle's Medium (DMEM) (Gibco/Life Technologies, Grand Island, NY, USA) supplemented with antibiotics (penicillin and streptomycin) and 10% fetal bovine serum (Gibco/Life Technologies) at 37 °C in the presence of 5% CO_2. For all the results showed in this study, EV-A71 infections were carried out at a multiplicity of infection (MOI) of 1. It was testified to be an appropriate viral dose for HeLa cells in our previous research, which ensured both cell status and rate of infection. According to the statistical results in confocal microscopy, the infection rates in the first 12 h ranged from 30% to 40% in different experiments.

Reagents and Antibodies

2-(4-Amidinophenyl)-6–indolecarba-midine dihydrochloride (DAPI) staining solution and the protease-inhibitor cocktail were purchased from Sigma Aldrich (St. Louis, MO, USA). MitoTrackerRed probes, TRIzol reagent and Lipofectamine 3000 were purchased from Invitrogen (Carlsbad, CA, USA). Nocodazole and Fluo-3 AM were purchased from Beyotime (Shanghai, China). Erythro-9-(2-hydroxy-3-nonyl) adenine (EHNA) and 2-Aminoethoxydiphenyl borate (2-APB) were purchased from Cayman Chemical (Ann Arbor, MI, USA). A23187 and thapsigargin were purchased from Abcam (Cambridge, MA, USA). N-dodecyl-D-maltoside (DDM) was purchased from Affymetrix. SB743921 was purchased from Selleck Chemicals (Houston, TX, USA). Ribavirin was purchased from Meryer (Shanghai, China). Mouse anti-EV-A71 VP1 monoclonal antibody was purchased from Merck Millipore (Billerica, MA, USA). Mouse anti-β tubulin monoclonal antibody, mouse anti-β actin monoclonal antibody, FITC-conjugated anti-mouse IgG antibody, HRP-conjugated anti-mouse IgG antibody and HRP-conjugated anti-rabbit IgG antibody were all purchased from Santa Cruz Biotechnology (Santa Cruz, CA, USA). Rabbit anti-VDAC and rabbit anti-syntaxin 6 monoclonal antibody was purchased from Cell Signaling Technology (Danvers, MA, USA). Mouse anti-RHOT1 monoclonal antibody was purchased from Abcam.

Immunofluorescence Confocal Microscopy and Flow Cytometry Analysis

For immunofluorescence confocal microscopy, cells were seeded onto coverslips and cultured overnight before infection, transfection or reagent treatments. Mitochondria were stained by using MitoTrackerRed (50 nmol/L) according to the manufacturer's instructions, followed by fixation with 4% paraformaldehyde for 30 min and permeabilization with 0.2% Triton X-100 for 20 min. The coverslips were then rinsed with phosphate-buffered saline (PBS, pH 7.4) and incubated with 5% (wt/vol) bovine serum albumin (BSA) in PBS for 1 h at room temperature to block any residual aldehyde groups. After 2 washes with PBS, the cells were incubated with the selected antibodies for 1.5 h at room temperature or 4 °C overnight. The cells were then washed thrice with PBS and incubated for 1 h with a fluorescence-conjugated second antibody. After washing thrice with PBS, cell nuclei were stained with DAPI and then mounted for microscopy. Fluorescence

images were acquired by confocal laser scanning microscopy (TCS SP8, Leica, Wetzlar, Germany).

For flow cytometry analysis, the cells were dissociated and harvested at the indicated times after being stained with 5 μmol/L Fluo-3 AM for 25 min. The cells were then washed 3 times with PBS and analyzed by using a flow cytometer (FACS Calibur, BD, San Jose, CA, USA).

RNA Extraction and RT-qPCR

Cellular total RNAs, including viral genome, were extracted from the infected cells harvested from each treatment using the TRIzol reagent (Life Technologies). Total RNAs (2 μg for each sample) were reverse-transcribed with a GoScript Reverse Transcriptase kit (Promega). Supernatants viral RNAs were isolated from 200 μL of the cell culture supernatants from each treatment using the TIANamp Virus DNA/RNA Kit (TIANGEN), reverse-transcribed, and tested in parallel in the same operation. A two-step RT-qPCR was performed in a SYBR Green assay in an ABI 7500 Real-Time PCR system using the GoTaq qPCR Master Mix reagents kit (Promega) and the EV-A71 sense primer 5′-AGTATGATTGAGACTCGGTG-3′ and antisense primer 5′-GCGACAAAAGTGAACTCTGC-3′ in the following amplification profile: one cycle at 95 °C for 10 min, 40 cycles, each of 95 °C for 10 s and 60 °C for 1 min. Viral RNA copy numbers were calculated automatically by the ABI 7500 Real-Time PCR system when the reaction finished.

Plasmid Construction and Protein Expression

To create the vectors expressing EV-A71 VP1, VP2, VP3, VP4, 2BC, 2B, 2C, 3AB, 3A, 3C or 3D proteins, EV-A71 genomic RNA was extracted from the culture supernatants of HeLa cells that were infected with EV-A71. Single-stranded cDNA was then synthesized from the purified virus RNA by reverse transcription (Promega, Madison, WI, USA). Each of the VP1, VP2, VP3, VP4, 2BC, 2B, 2C, 3AB, 3A, 3C and 3D genes was amplified from the cDNA by PCR over 34 cycles of denaturation at 98 °C for 10 s, primer annealing at 58 °C for 30 s and extension at 72 °C for 1.5 min, using primers listed in Supplementary Table S1. Each of the PCR products was separated by electrophoresis in 1.0% agarose gel, purified and then cloned into the corresponding restriction sites of the pcDNA3.0-EGFP or pcDNA3.0-Flag vector after being digested with *Bam*H I and *Eco*R I or *Hin*d III and *Sal* I, respectively. The recombinant plasmids were sequenced and then transfected separately into HeLa cells using Lipofectamine 3000 according to the manufacturer's instructions. The expression of each protein was confirmed by Western blotting (WB) analysis.

Protein Extraction and Western Blotting

Cultured cells for protein extraction were collected and washed three times with PBS. After centrifugation at 500 $\times g$, the cell pellets were resuspended in cell lysis buffer (0.3% DDM in PBS) containing the protease inhibitor cocktail and incubated on ice for 30 min. Supernatants and pellets were collected after centrifugation at 14,000 $\times g$ for 10 min at 4 °C. For WB, the samples were heat-denatured in sample-loading buffer (50 mmol/L Tris–HCl, pH 6.8, 100 mmol/L DTT, 2% SDS, 0.1% bromophenol blue and 10% glycerol) for 10 min and separated by SDS–polyacrylamide gel electrophoresis (12% polyacrylamide, 0.1% SDS) and then transferred onto polyvinylidene fluoride membranes (Millipore) for WB analysis. The membranes were blocked with 5% skim milk in TBST buffer (50 mmol/L Tris–HCl, 100 mmol/L NaCl and 0.1% Tween-20, pH 7.4) for 1 h at 20 °C and then incubated with the indicated primary antibodies for 90 min at 20 °C. After three washes with TBST buffer, the membranes were incubated with the corresponding HRP-conjugated secondary antibody for 45 min at room temperature. The signals on the membranes were detected by the ELC (Millipore) method.

Mitochondria Purification and Fractionation

Mitochondria were isolated using a Cell Mitochondria Isolation Kit (Beyotime) as described in the instructions. In brief, the cells were collected and washed three times with PBS. After centrifugation at 500 $\times g$ for 5 min, the pellets were resuspended in 500 μL of cold mitochondria isolation buffer consisting of 0.3 mol/L sucrose, 1 mmol/L EGTA, 5 mmol/L morpholinopropanesulfonic acid (MOPS), 5 mmol/L KH_2PO_4 and 0.1% (wt/vol) BSA (pH 7.5) in the presence of protease inhibitors and then homogenized in a glass homogenizer. The disrupted cells were centrifuged at 1000 $\times g$ for 10 min to pellet the unlysed cells and nuclei. The supernatants were centrifuged further at 11,000 $\times g$ for 20 min at 4 °C to obtain the crude mitochondria fractions.

Pull-down Assay and Co-immunoprecipitation

The protein A/G-agarose beads were washed three times with PBS and once with lysis buffer (0.3% DDM in PBS) before use. Cultured cells were washed twice with PBS and incubated with ice-cold cell lysis buffer containing the protease inhibitor cocktail for 5 min. Cells were then scrape off the dish with cell scrapers, transferred into centrifuge tubes and incubated on ice for 30 min. After centrifugation at 14,000 $\times g$ for 10 min at 4 °C, the

supernatants of the cell lysates were pre-cleared by incubating with protein A/G-agarose beads at 4 °C for 10 min on a rotator. The protein A/G-agarose beads were then removed by centrifugation at 14,000 ×*g* for 5 min. The cell lysates were incubated with the anti-RHOT1 monoclonal antibody and gently rotated for 2 h at 4 °C. The lysate-antibody compounds were then captured by incubating with protein A/G agarose beads and gently rotated for 2 h at 4 °C. After washing three times with PBS, the incubated beads were boiled and the proteins in the supernatants were collected and subjected to WB analysis.

siRNAs and Knockdown Experiment

Small interfering RNAs (siRNAs) that target human RHOT1 and non-targeting negative control siRNA (Nc-si) were chemically synthesized. Transient transfections using Lipofectamine 3000 were conducted according to the manufacturer's instructions. At 48 h after transfection, HeLa cells were detached and subcultured to new dishes for subsequent experiments. Gene silencing with siRNA was verified by detecting the mRNA levels by RT-qPCR.

Statistical Analysis

Data were subjected to one-way analysis of variance with factors of treatments and expressed as means ± standard deviations. Comparisons between any two groups were performed by unpaired Student's *t* tests. * indicates a significant difference at *P* values of 0.01 compared to the control. ** indicates a significant difference at *P* values of 0.001 compared to the control.

Results

Perinuclear Clustering of Mitochondria during EV-A71 Infection

To investigate whether EV-A71 infection alters the subcellular localization of mitochondria, HeLa cells were infected with EV-A71 in the indicated times and stained with the mitochondrion-specific fluorescent dye MitoTrackerRed. EV-A71 virions and nuclei were marked by staining respectively with the anti-EV-A71 VP1 antibody and DAPI after fixation and permeabilization. The results of confocal microscopy in Fig. 1A showed that the mitochondria were spread throughout the cytoplasm in the uninfected cells. In comparison, the mitochondria in EV-A71-infected cells began to migrate to the area around nucleus at 4 h post-infection (hpi). After 8 hpi, almost all the mitochondria were found to aggregate at the perinuclear site. In the cells infected in the presence of 500 μmol/L of ribavirin (antiviral drug), the mitochondria redistribution and EV-A71 specific fluorescence signal were not observed until 8 hpi and the mitochondria were found to totally aggregate by 12 hpi. To make sure that the mitochondria redistribution was not caused by cytopathic effect (CPE), the cell morphology change was monitored by microscopy. As shown in Fig. 1B, the EV-A71-infected cells began to shrink slightly at 12 hpi and turned round by 16 hpi, but no obvious CPE was observed before 8 hpi.

We then analyzed the virus replication by detecting the viral RNA in both the infected cells and the culture supernatants by RT-qPCR. The results in Fig. 1C showed that the viral RNA in the EV-A71-infected cells was dramatically increased in the first 8 h of infection. In consistent with the result of confocal microscopic analysis, virus replication was significantly inhibited by ribavirin. The treatment of ribavirin reduced the viral RNA level by 71% at 4 hpi and 55% at 8 hpi, respectively. On the other hand, there was hardly any virus release before 12 hpi, indicating that there was no destruction of the infected cells in the first 12 h of infection.

To quantify the impact of EV-A71 infection on mitochondria redistribution, the mitochondria-occupied areas in the cells at different times post infection were calculated

Fig. 1 EV-A71 infection induces the perinuclear clustering of mitochondria. **A** Confocal microscopy analysis of the localization of mitochondria in EV-A71-infected HeLa cells. Cells were infected with EV-A71 for 4 h, 8 h or 12 h, either in the presence or absence of 500 μmol/L of ribavirin. The cells were then stained respectively with the anti-EV-A71 VP1 antibody (green), MitoTrackerRed (red) and DAPI (blue). The overlaid images of three fluorescences were shown. The scale bar indicates 10 μm. Mock: Uninfected cells. **B** Morphological changes observed in EV-A71-infected HeLa cells by bright-field microscopy at 4, 8, 12, 16, 20 and 24 hpi. The scale bar indicates 20 μm. Mock: Uninfected cells. **C** Measurements of viral RNA levels in the EV-A71-infected HeLa cells and culture supernatants by absolute quantitative RT-qPCR. Cells were infected with EV-A71, either in the presence or absence of 500 μmol/L of ribavirin for 4 h, 8 h, 12 h, 16 h, 20 h or 24 h. Total RNA in the infected cells and viral genome in the supernatants were extracted and reverse-transcripted as described in "Materials and Methods" section. "Copies of viral RNA" represents the number of EV-A71 genomic RNA copies in 100 ng of total RNA from the infected cells (left) or 1 μL of the culture supernatant (right). **D** Quantification of mitochondria-occupied areas in EV-A71-infected HeLa cells. HeLa cells, uninfected (left) or infected with EV-A71 (right) were respectively stained with the anti-EV-A71 VP1 antibody (green), MitoTrackerRed (red) and DAPI (blue). The areas occupied by nucleus (N), mitochondria (M) and the whole cell (C) were outlined respectively with white, yellow or green lines and calculated by using the Leica Application Suite Advanced Fluorescence. The area of the nucleus was always included in the calculation of mitochondira area (M). The proportion of mitochondria in the cytoplasmic area [(M−N)/(C−N)] was used as a measure of the degree of mitochondria clustering in the nuclear periphery. Data of the means ± standard deviations for the different infection times are shown on the right. For each sample, 30 cells were counted.

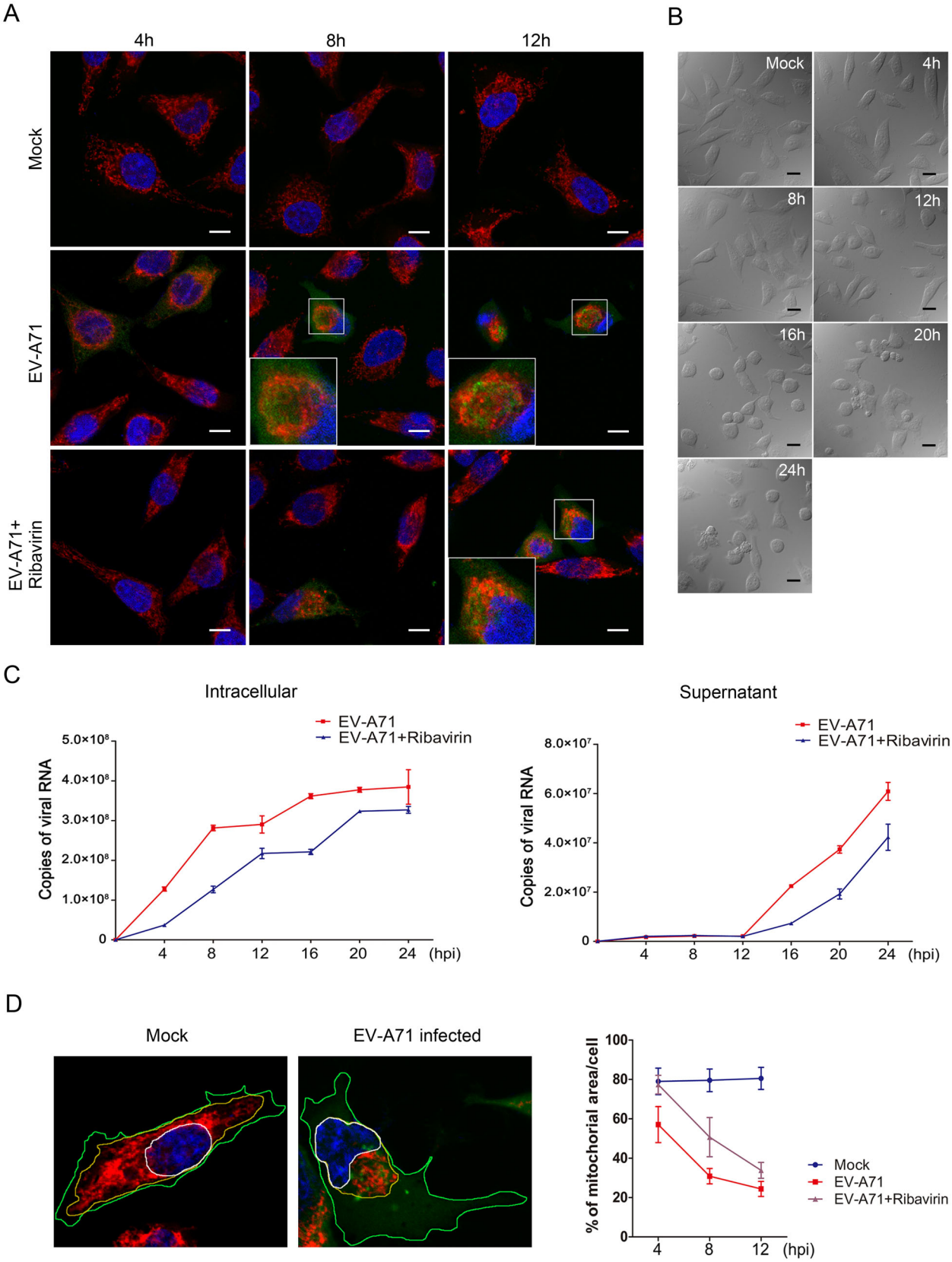
A
4h
8h
12h
Mock
EV-A71
EV-A71+ Ribavirin
B
Mock
4h
8h
12h
16h
20h
24h
C
Intracellular
EV-A71
EV-A71+Ribavirin
Copies of viral RNA
5.0×10⁸
4.0×10⁸
3.0×10⁸
2.0×10⁸
1.0×10⁸
0
4 8 12 16 20 24 (hpi)
Supernatant
EV-A71
EV-A71+Ribavirin
Copies of viral RNA
8.0×10⁷
6.0×10⁷
4.0×10⁷
2.0×10⁷
0
4 8 12 16 20 24 (hpi)
D
Mock
EV-A71 infected
% of mitochorial area/cell
100
80
60
40
20
0
4 8 12 (hpi)
Mock
EV-A71
EV-A71+Ribavirin

(Fig. 1D). Thirty cells were counted for each sample. In cells with no EV-A71 infection, the mean percentage of cell areas occupied by mitochondria was about 80% and no obvious change was observed by increasing the time of culture. In comparison, the mitochondria areas in the cells infected with EV-A71 for 4 h, 8 h and 12 h were reduced to 57%, 30.8% and 24.4%, respectively. However, in the EV-A71-infected cells that were treated with ribavirin, the mitochondria areas were 77.3%, 50.7% and 33.8% at the indicated times post infection. The above results showed that the mitochondria clustering and viral RNA level in cells increased dramatically at the same time. When virus replication was suppressed by ribavirin, the mitochondria migration was postponed correspondingly, suggesting that the perinuclear mitochondria aggregation was synchronized with virus replication. These results indicated that EV-A71 infection caused the mitochondria to aggregate at the perinuclear sites which might be the EV-A71 replication center.

Involvement of the Microtubule Network and the Dynein Complex in EV-A71-induced Mitochondria Redistribution

Mitochondria transport in cells involves mainly two kinds of cytoskeletons, microtubules and microfilaments (Hollenbeck and Saxton 2005). To investigate the roles of microtubules and microfilaments in mitochondria redistribution in EV-A71 infections, infected HeLa cells were treated with nocodazole (a microtubule-destabilizing reagent) or cytochalasin D (an actin polymerization inhibitor). The microtubule and microfilament structures were found to disappear in HeLa cells treated with either 10 μmol/L of nocodazole or 1 μmol/L of cytochalasin D for 1.5 h, respectively, indicating that these agents were capable of depolymerizing these cytoskeletons at these concentrations (Fig. 2A). As shown in Fig. 2B, the depolymerization of microtubules by nocodazole resulted in a complete abolishment of mitochondria aggregation in all the treated cells. In contrast, the mitochondria remained aggregated in cells treated with cytochalasin D. EV-A71-infected cells with no nocodazole or cytochalasin D treatment showed obvious mitochondria clustering. In comparison, the mitochondria remained dispersed in the corresponding treated uninfected cells. The above results demonstrated that microtubules, but not microfilaments, were involved in mitochondria redistribution in the EV-A71-infected cells.

The transport of organelles along the microtubule is carried out by two motor proteins, kinesin and dynein. Kinesin is responsible for the transport of organelles toward the plasma membrane, whereas dynein is responsible for organelles movement toward the nucleus or the MTOC (Dixit *et al.* 2008). Thus, dynein possibly participates in EV-A71-induced perinuclear mitochondria migration. To examine this, EV-A71-infected HeLa cells were treated with EHNA (an inhibitor of dynein ATPase) and SB743921 (an inhibitor of kinesin) and then subjected to confocal microscopy. In the above study, the perinuclear migration of mitochondria was observed as early as 4 hpi. To abolish the migration, EHNA and SB743921 were added into the culture medium at 2 hpi. As shown in Fig. 2B, in comparison with the infected cells untreated or treated with 10 nmol/L of SB743921, the cells treated with 0.5 mmol/L of EHNA almost completely suppressed the perinuclear clustering of mitochondria, indicating that the dynein motor activity was crucial for EV-A71-induced mitochondria migration.

We then analyzed the mitochondria-occupied areas in the cells with the treatments mentioned above. As shown in Fig. 2C, the mitochondria area in cells infected with EV-A71 for 8 h was 31.5%. However, EV-A71-infected cells treated with either 10 μmol/L of nocodazole at 6.5 hpi or 0.5 mmol/L of EHNA at 2 hpi restored the mitochondria areas back to 78.1% and 73.0%, respectively. In contrast, in the infected cells treated with 1 μmol/L of cytochalasin D for 1.5 h or 10 nmol/L of SB743921 for 6 h, the mitochondria areas were 31.6% and 30.1%, both of which were not significantly different from those of the untreated infected cells. The mitochondria areas in the uninfected cells with the above treatments remained at 75%–80%. Collectively, these results revealed that the microtubule skeleton and the dynein motor complex were required for mitochondria redistribution in the EV-A71-infected cells.

Effect of Cytoplasmic Calcium Concentration on Mitochondria Redistribution in the EV-A71-infected Cells

It was reported that mitochondrial motility was regulated by calcium concentration ($[Ca^{2+}]_c$). Mitochondria transport can proceed at resting levels of $[Ca^{2+}]_c$, while an increase in $[Ca^{2+}]_c$ will attenuate and even completely abolish mitochondria movement. That provides a mechanism to recruit and keep mitochondria to the Ca^{2+} release sites (Yi *et al.* 2004). Thus, we hypothesized that EV-A71 infection may induce mitochondria clustering by regulating intracellular $[Ca^{2+}]_c$. We then examined the change of cytoplasmic $[Ca^{2+}]_c$ in the infected HeLa cells. The cells were stained with Fluo-3 AM at the indicated times post infection and subjected to flow cytometry analysis. As shown in Fig. 3A, no significant difference in cytoplasmic $[Ca^{2+}]_c$ was detected between the uninfected HeLa cells and those infected with EV-A71, suggesting that EV-A71 has no obvious influence on cytoplasmic $[Ca^{2+}]_c$ of the host cells.

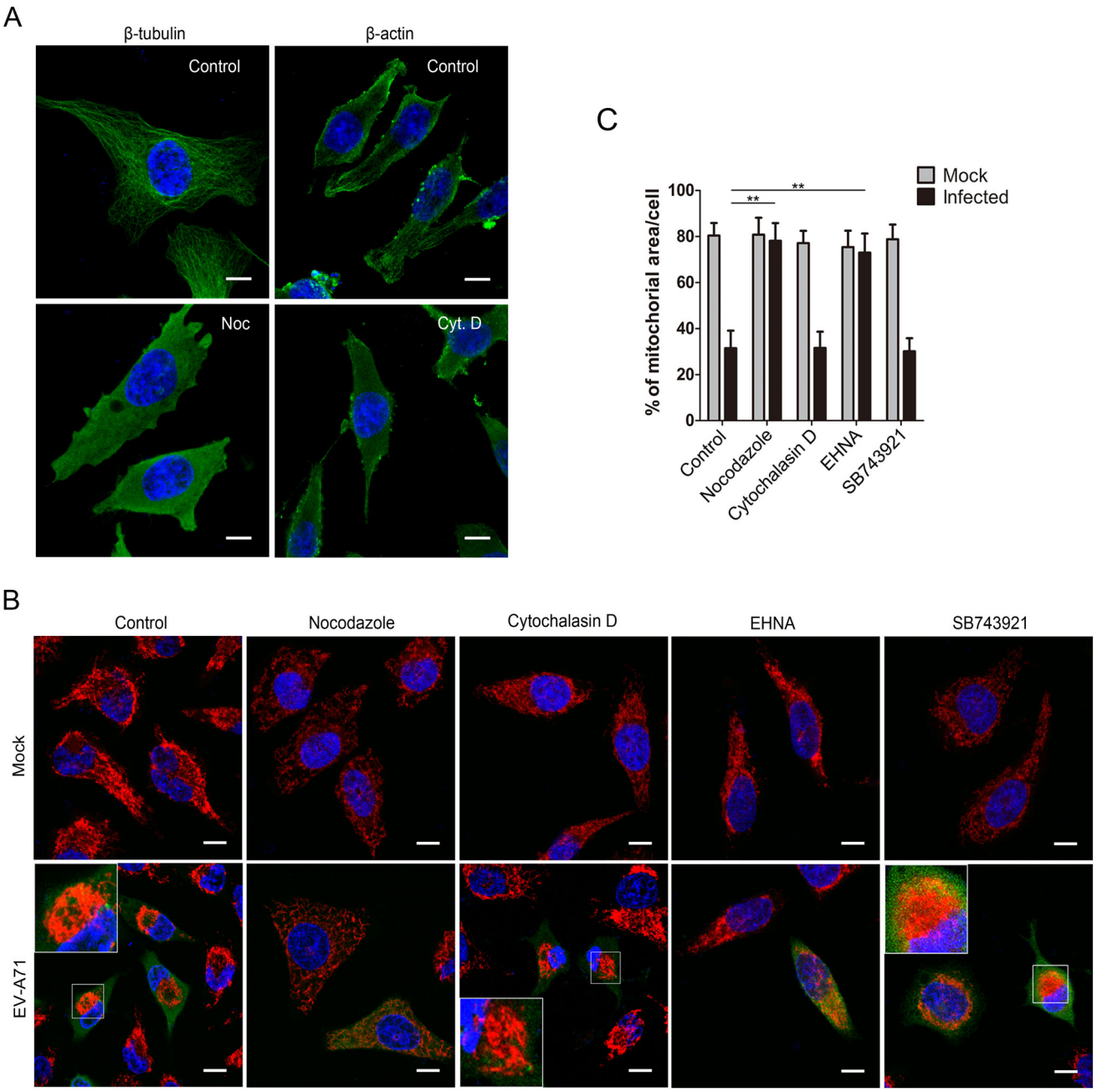

Fig. 2 Microtubule network and dynein complex are crucial for EV-A71-induced mitochondria redistribution. **A** Identification of depolymerization effect of nocodazole and cytocalasin D on microtubules and microfilaments. HeLa cells were treated with either 10 μmol/L of nocodazole (Noc) or 1 μmol/L of cytochalasin D (Cyt. D) for 1.5 h. The cells were then stained with either anti-β tubulin (left) or anti-β actin (right) antibody and DAPI. Control: DMSO treated cells. **B** Confocal microscopy analysis of the localization of mitochondria in the EV-A71-infected cells with different treatments. HeLa cells were infected with EV-A71 for a total of 8 h and treated respectively as mentioned below. Cells were then stained respectively with the anti-EV-A71 VP1 antibody (green), MitoTrackerRed (red) and DAPI (blue). The overlaid images of three fluorescences were shown. Nocodazole: infected cells were incubated with 10 μmol/L of nocodazole at 6.5 hpi for 1.5 h. Cytochalasin D: infected cells were incubated with 1 μmol/L of cytochalasin D at 6.5 hpi for 1.5 h. EHNA: infected cells were incubated with 0.5 mmol/L of EHNA at 2 hpi for 6 h. SB743921: infected cells were incubated with 10 nmol/L of SB743921 at 2 hpi for 6 h. Mock: uninfected HeLa cells. Control: cells treated with DMSO. The scale bar indicates 10 μm. **C** Quantification of mitochondria-occupied areas in the EV-A71-infected HeLa cells. The indicated proportions of mitochondria areas in the cytoplasms were marked and calculated as described above. The data were shown as the means±standard deviations for the corresponding different treatments (**$P<0.001$ by Student's t test). For each sample, 30 cells were counted.

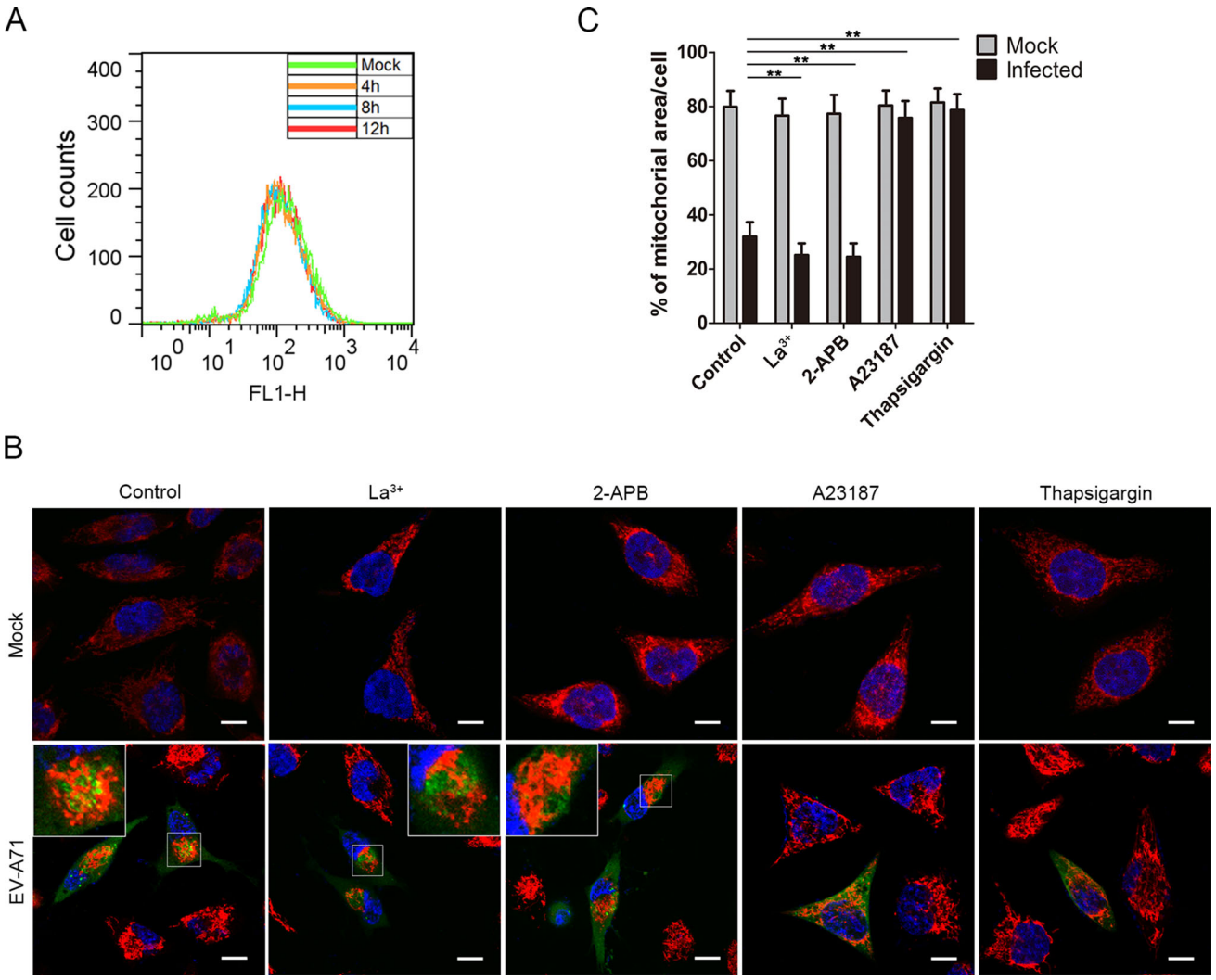

Fig. 3 Mitochondria redistribution in the EV-A71 infected cells is regulated by cytoplasimic calcium concentration. **A** Flow cytometry analysis of cytoplasmic calcium concentrations ($[Ca^{2+}]_c$) in HeLa cells infected with EV-A71. Uninfected HeLa cells (Mock) and HeLa cells infected for 4 h, 8 h or 12 h were stained with Fluo-3 AM and subject to flow cytometry analysis. **B** Confocal microscopy analysis of the localizations of mitochondria in EV-A71-infected HeLa cells treated with Ca^{2+} regulating agents. HeLa cells were infected with EV-A71 for 8 h in the presence of either La^{3+} (15 μmol/L), 2-APB (75 μmol/L), A23187 (2 μmol/L) or thapsigargin (2 μmol/L). The cells were then stained respectively with the anti-EV-A71 VP1 antibody (green), MitoTrackerRed (red) and DAPI (blue). The overlaid images of three fluorescences were shown. Mock: uninfected HeLa cells. Control: cells treated with DMSO. The scale bar indicates 10 μm. **C** Quantification of mitochondria-occupied areas in the EV-A71-infected HeLa cells. The indicated proportions of mitochondria areas in the cytoplasms were marked and calculated as described above. The shown data were the means ± standard deviations for the corresponding different treatments (**$P < 0.001$ by Student's t test). For each sample, 30 cells were counted.

We also analyzed the distributions of mitochondria in the infected cells treated with different Ca^{2+} regulating agents. HeLa cells were infected with EV-A71 in the presence of either 15 μmol/L of lanthanum iron (La^{3+}), 75 μmol/L of 2-APB, 2 μmol/L of A23187 or 2 μmol/L of thapsigargin for 8 h. As shown in Fig. 3B, the mitochondria remained clustered in the infected cells treated with La^{3+} or 2-APB, both of which were capable of reducing the cytoplasmic $[Ca^{2+}]_c$. However, the infected cells treated with A23187 or thapsigargin, agents known to raise cytosolic $[Ca^{2+}]_c$, showed no mitochondria clustering. The mitochondria in the uninfected cells with the above treatments also remained dispersed. These results indicated that the EV-A71-induced mitochondria aggregation was suppressed under a high cytoplasmic $[Ca^{2+}]_c$ environment.

Additionally, as shown in Fig. 3C, measurements of the mitochondria-occupied areas in these cells suggested that the mitochondria aggregation in the La^{3+}-(25.2%) and 2-APB-(24.5%) treated cells were even stronger than that of the infected control cells (31.9%) at 8 hpi, indicating that reducing the cytosolic $[Ca^{2+}]_c$ might facilitate mitochondria clustering. In comparison, the treatment with

A23187 or thapsigargin kept the mitochondria areas in the infected cells at 75.8% or 78.6%, respectively, which was not significantly different from those of the uninfected cells (76%–81%). Taken together, these results suggested that a low cytoplasmic $[Ca^{2+}]_c$ was essential for the mitochondria redistribution induced by EV-A71 infection.

Induction of Mitochondria Redistribution by the EV-A71 Nonstructural Protein 2BC

To identify the EV-A71 proteins that were responsible for the mitochondria aggregation, plasmids that expressed each of the EV-A71 VP1, VP2, VP3, VP4, 2BC, 2B, 2C, 3A, 3C or 3D proteins with an EGFP tag were constructed and transfected separately into HeLa cells which were then analyzed by confocal microscopy. As shown in Fig. 4A, typical mitochondria aggregation was observed only in cells expressing the nonstructural precursor protein 2BC. In comparison, the mitochondria were dispersed within the cytoplasm of cells expressing either EGFP or any of the other EV-A71 structural and nonstructural proteins, including the 2BC cleavage products, 2B and 2C.

To compare the characteristics of the EV-A71-induced and 2BC-induced mitochondria redistribution, similar treatments were performed in cells with 2BC expression. As the confocal microscopy results, shown in Fig. 4B, the mitochondria redistribution in the 2BC-expressing cells was blocked by either nocodazole, EHNA, A23187 or thapsigargin treatments. In contrast, the mitochondria remained clustered in the cells treated with either cytochalasin D, SB743921, 2-APB or La^{3+} as well as in the untreated 2BC-expressing cells. There was no obvious change in mitochondria distribution in the cells expressing EGFP under the same treatments. Collectively, these results indicated that the 2BC-induced mitochondria redistribution depended on a complete microtubule network, functional dynein complexes and a low cytoplasmic $[Ca^{2+}]_c$, which was consistent with that induced by EV-A71 infection.

Cellular Localization of EV-A71 2BC Protein and Its Interaction with the Mitochondrial Protein RHOT1

As indicated by confocal microscopy, a higher concentration of the viral nonstructural protein 2BC was observed in the area where mitochondria were aggregating (Fig. 5A). To investigate the relationship between 2BC and the mitochondria, mitochondrial fractions of HeLa cells transfected with either the pcDNA3.0-2BC-Flag or pcDNA3.0-Flag vector were isolated. Equal amounts of proteins from the cytosol, mitochondria and whole cell lysate were resolved by SDS-PAGE followed by immunoblotting with the anti-Flag antibody. Western blot analysis showed that almost all of the 2BC protein was present in the mitochondrial fractions and almost undetectable in the cytosol of HeLa cells, suggesting that the majority of the EV-A71 2BC protein was located on the mitochondria (Fig. 5B). To examine the purification of the mitochondrial fractions, voltage-dependent anion-selective channel (VDAC, a marker of mitochondria) and syntaxin 6 (a marker of Golgi apparatus) were separately probed. The results confirmed the purity of mitochondrial fractions.

Mitochondrial Rho GTPase 1 (RHOT1, also known as MIRO1) is a key protein involved in mitochondria movement and is located on the outer membrane of the mitochondria. It facilitates mitochondria transport by attaching the mitochondria to motor proteins and regulates it by binding Ca^{2+} and abolishes this attachment at high $[Ca^{2+}]_c$ levels (Liu and Hajnoczky 2009). Given that 2BC and RHOT1 share a similar subcellular localization and a related function in mitochondrial motility, we hypothesized that the viral nonstructural protein 2BC may induce mitochondria aggregation by interacting with RHOT1. Co-immunoprecipitation assays were performed with cells expressing the EGFP-tagged 2BC, 2B or 2C protein. As shown in Fig. 5C, antibodies against RHOT1 co-precipitated with RHOT1 and the 2BC protein, indicating that there was an interaction between the 2BC protein and RHOT1. However, neither the 2B nor 2C protein co-precipitated with RHOT1. The results above provided a potential mechanism for the EV-A71 to induce mitochondria redistribution via the 2BC protein.

Restriction of Mitochondria Redistribution and Its Effect on EV-A71 Replication

To evaluate the roles of mitochondria redistribution during EV-A71 replication, HeLa cells were infected with EV-A71 in the presence of either nocodazole, EHNA, A23187, thapsigargin, 2-APB or La^{3+} and harvested at 24 hpi. Cell lysates containing equal amounts of proteins were subjected to Western blotting analysis and probed by the anti-EV-A71 VP1 antibody to detect the virion protein levels. As shown in Fig. 6A, the amounts of virus in the cells treated with either nocodazole, EHNA, thapsigargin or A23187 were decreased, but not in the cells treated with either 2-APB or La^{3+}, indicating that the treatments that suppress the mitochondria clustering had resulted in a decrease in virus replication. RT-qPCR was then performed to determine the levels of viral RNA in the infected cells and culture supernatants. The results in Fig. 6B showed that nocodazole, EHNA, thapsigargin and A23187 treatments reduced the number of copies of EV-A71 RNA significantly in both the cytosol and culture supernatant fractions of the treated cells, while 2-APB and La^{3+}

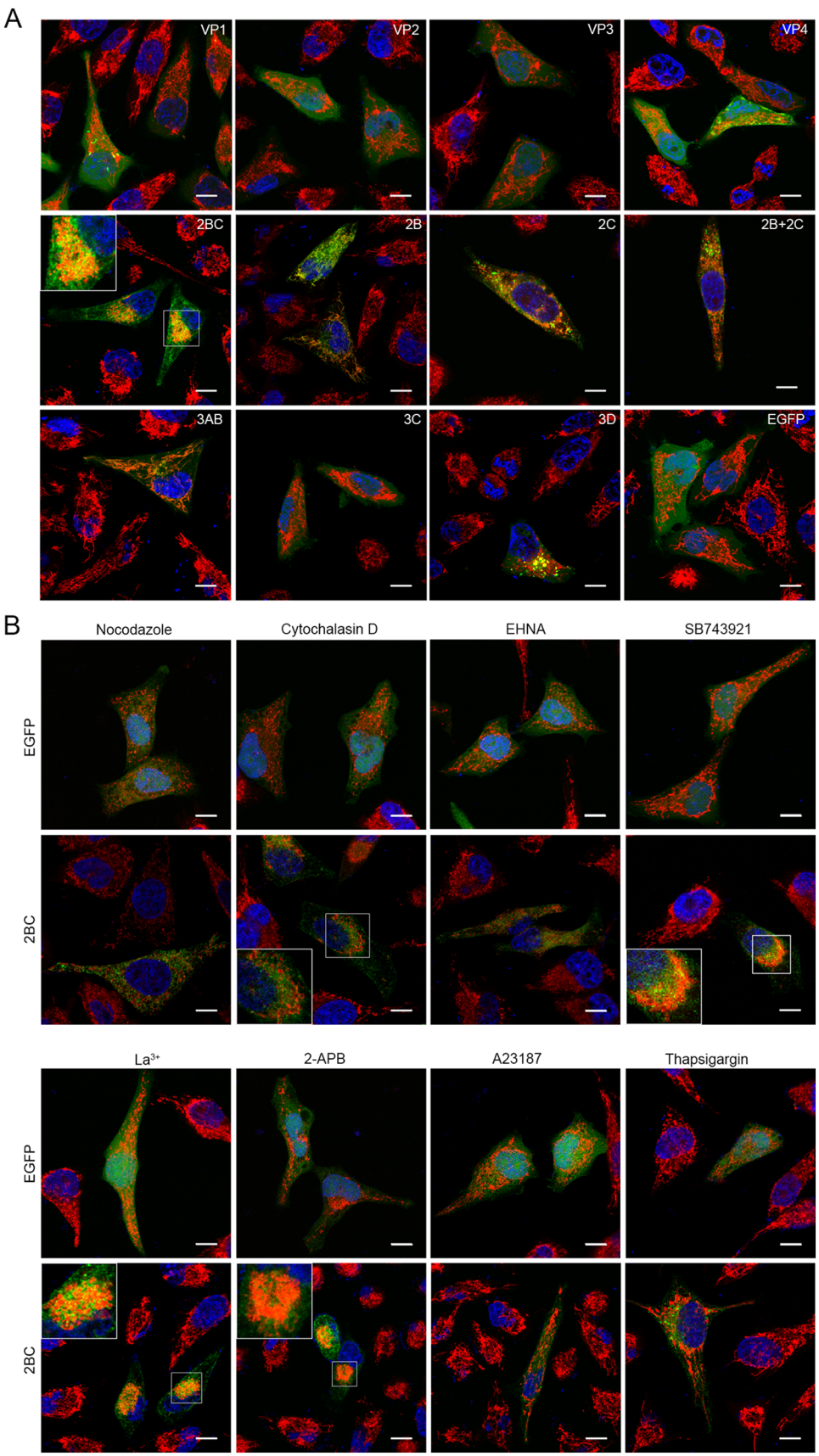

Fig. 4 Viral protein 2BC induces the redistribution of mitochondria. **A** Confocal microscopy analysis of the localizations of mitochondria in HeLa cells expressing the different EV-A71 proteins. HeLa cells were transfected with the respective plasmids expressing either EGFP or the different viral proteins and cultured for 12 h. The cells were then stained respectively with MitoTrackerRed (red) and DAPI (blue). The overlaid images of three fluorescences were shown. The scale bar indicates 10 μm. **B** Confocal microscopy analyses of HeLa cells transfected with pcDNA3.0-EGFP or pcDNA3.0-2BC-EGFP for 12 h and treated respectively as mentioned below. The cells were then stained as described above. The overlaid images of three fluorescences were shown. Nocodazole: cells were transfected for 10.5 h and incubated with 10 μmol/L of nocodazole for another 1.5 h. Cytochalasin D: cells were transfected for 10.5 h and incubated with 1 μmol/L of cytochalasin D for another 1.5 h. EHNA: cells were transfected for 2 h and incubated with 0.5 mmol/L of EHNA for another 10 h. SB743921: cells were transfected for 2 h and incubated with 10 nmol/L of SB743921 for another 10 h. La^{3+}: cells were transfected for 2 h and incubated with 15 μmol/L of La^{3+} for another 10 h. 2-APB: cells were transfected for 2 h and incubated with 75 μmol/L of 2-APB for another 10 h. A23187: cells were transfected for 2 h and incubated with 2 μmol/L of A23187 for another 10 h. Thapsigargin: cells were transfected for 2 h and incubated with 2 μmol/L of thapsigargin for another 10 h. Control: cells treated with DMSO. The scale bar indicates 10 μm.

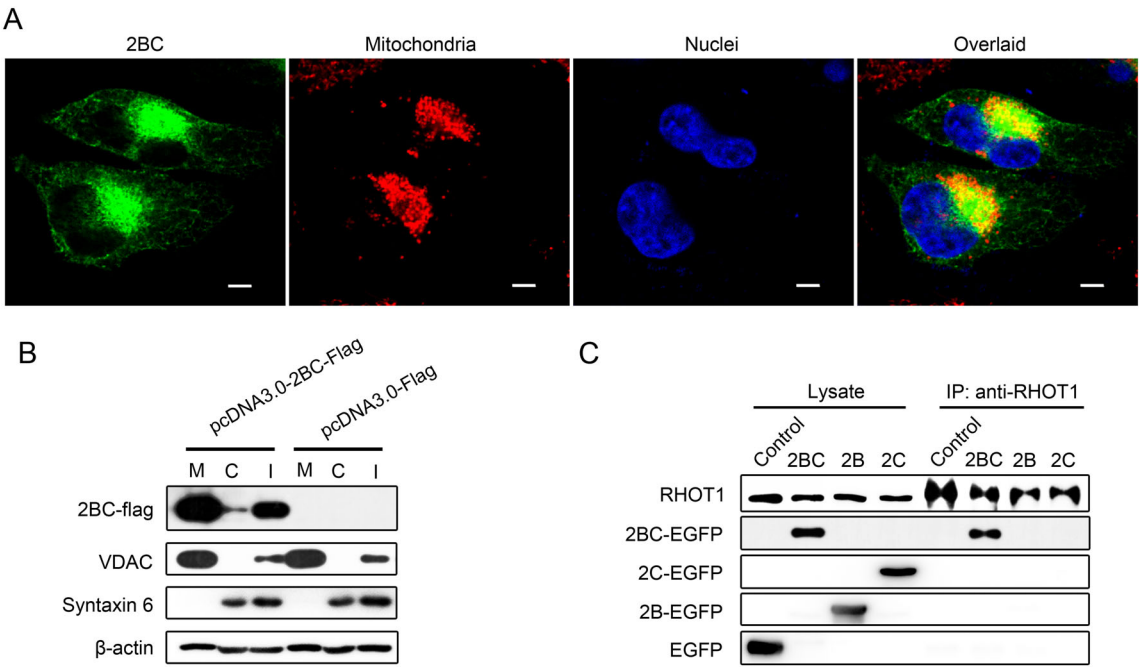

Fig. 5 EV-A71 2BC protein is located on the mitochondria and interacts with RHOT1. **A** Confocal microscopy analysis of the subcellular localization of 2BC in HeLa cells. Cells transfected with pcDNA3.0-2BC-EGFP were stained respectively with MitoTrackerRed (red) and DAPI (blue). Images of each stained component and the corresponding overlaid image were shown respectively. The scale bar indicates 5 μm. **B** Western blotting analysis of 2BC protein in the cytosolic and mitochondrial fractions of HeLa cells that were transfected with either pcDNA3.0-2BC-Flag or pcDNA3.0-Flag. Cytosolic and mitochondrial fractions were separated as described in "Materials and Methods" section and processed for immunoblotting with antibodies targeting Flag-tag, VDAC (a marker for the mitochondria), syntaxin 6 (a marker for the Golgi apparatus) and beta-actin. M: mitochondrial fractions. C: cytosolic fractions. I: cell lysates. **C** Detection of the specific interactions between 2BC and cellular RHOT1 in cell lysates by immunoprecipitation (IP) assays and Western blotting (WB). Cells were respectively transfected with either pcDNA3.0-EGFP (Control), pcDNA3.0-2BC-EGFP (2BC), pcDNA3.0-2B-EGFP (2B) or pcDNA3.0-2C-EGFP (2C). At 12 h post transfecion, the cells were harvested and subjected to immunoprecipitation. The different fractions were probed with anti-RHOT1 and GFP antibodies.

treatments had little impact. However, neither 2-APB nor La^{3+} treatment increased virus replication.

Besides, compared with the negative control (Nc-si), the number of copies of EV-A71 RNA were also reduced in both the infected cells and culture supernatants when the host cells were transfected with siRNA targeting RHOT1 (Fig. 6C, 6D). Collectively, these results indicated that mitochondria redistribution played a crucial role in EV-A71 replication and proliferation.

Discussion

The results presented in this study revealed that the redistribution of mitochondria in EV-A71 infected cells was essential for the life cycle of the virus. Importantly, it indicated that the EV-A71 2BC protein interacted with RHOT1 and played a crucial role in the regulation of mitochondrial motility. The schematic diagram in Fig. 7 shows a possible scenario for the mitochondria aggregation process in EV-A71-infected cells. Mitochondria movement is normally associated with microtubule at the outer region of the cytoplasm. When mitochondria are transported to the perinuclear region by dynein, the RHOT1 on the outer membrane of the mitochondria would bind to the newly translated 2BC protein at the EV-A71 replication center. Such binding might induce a conformation change or a site blockage on the RHOT1 that prevents the mitochondria from attaching to any other motor proteins and being transferred elsewhere. As a result, the mitochondria remain in place and accumulate at the EV-A71 replication centers.

The poliovirus (PV) and Coxsackie B virus (CVB) were reported to release Ca^{2+} from the endoplasmic reticulum (ER) and elevate cytosolic $[Ca^{2+}]_c$ by increasing the ER permeability through viroporin 2B (van Kuppeveld *et al.* 1997; Campanella *et al.* 2004; de Jong *et al.* 2006, 2008; Brisac *et al.* 2010). Although, interestingly, no significant change in the cytosolic $[Ca^{2+}]_c$ was observed in this study, there was still the possibility that EV-A71 induced the mitochondria aggregation by changing the local $[Ca^{2+}]_c$, without an obvious change in the overall $[Ca^{2+}]_c$ level. Since mitochondrial motility was negatively regulated by $[Ca^{2+}]_c$, the mitochondria would move along the $[Ca^{2+}]_c$

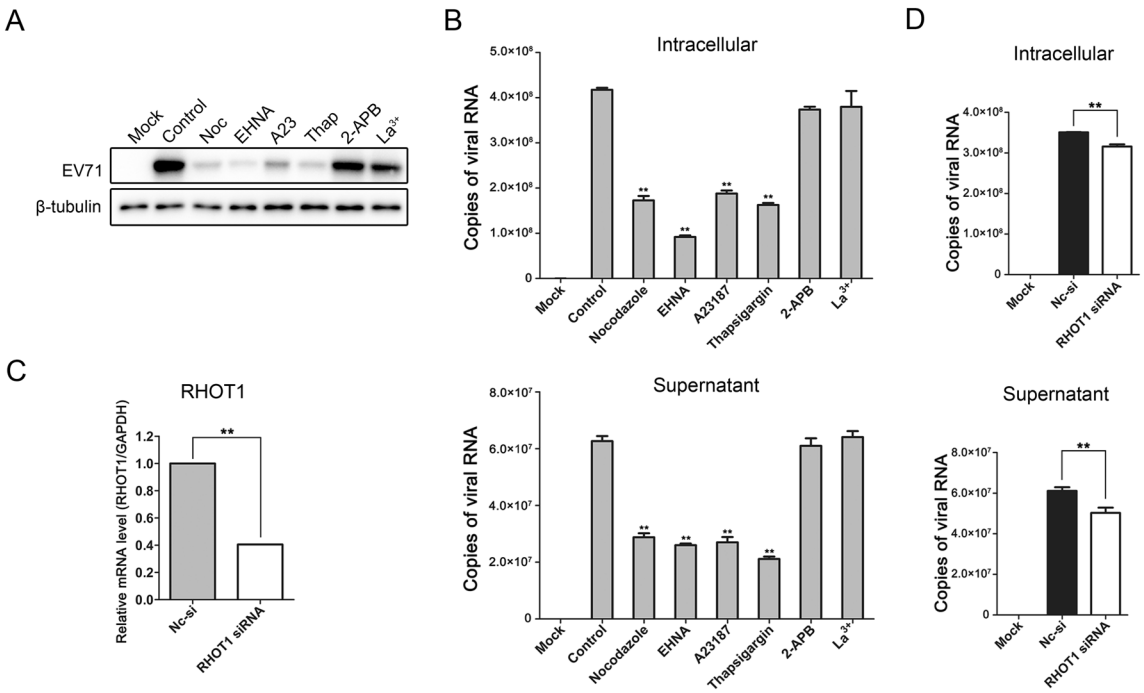

Fig. 6 Effects of mitochondria redistribution on EV-A71 replication. **A** Western blotting analysis of virus replication in HeLa cells infected with EV-A71 in the presence of either 10 μmol/L of nocodazole, 0.5 mmol/L of EHNA, 2 μmol/L of A23187 (A23), 2 μmol/L of thapsigargin (Thap), 75 μmol/L of 2-APB or 15 μmol/L of La^{3+}. The infected cells were harvested at 24 hpi and subjected to Western blotting with the anti-EV-A71 VP1 and beta-tubulin antibodies. Mock: uninfected HeLa cells. Control: EV-A71 infected cells treated with DMSO. **B** Measurements of viral RNA levels in the EV-A71-infected HeLa cells and culture supernatants with different treatments by absolute quantitative RT-qPCR. The cells were infected with EV-A71 for 24 h and treated as mentioned above. Total RNA in the infected cells and viral genome the in supernatants were extracted and reverse-transcripted as described in "Materials and Methods" section. "Copies of viral RNA" represents the number of EV-A71 genomic RNA copies in 100 ng of total RNA from the infected cells (top panel) or 1 μL of the culture supernatant (bottom panel). Mock: uninfected HeLa cells. Control: EV-A71-infected cells treated with DMSO. **C**, **D** RT-qPCR analysis of RHOT1 gene expression and EV-A71 replication in the HeLa cells that were transfected with siRNA targeting RHOT1. Cells were transfected with the siRNA targeting RHOT1 or the non-targeting negative control siRNA (Nc-si) for 48 h and then subcultured and cultivated for another 24 h. The cells were then infected with EV-A71 for 24 h. Total RNA in the infected cells and viral genome in the supernatants were extracted and reverse-transcripted as described in "Materials and Methods" section. RHOT1 mRNA levels were measured by relative quantitative RT-qPCR (**C**). EV-A71 RNA levels were measured by absolute quantitative RT-qPCR (**D**). "Copies of viral RNA" represents the number of EV-A71 genomic RNA copies in 100 ng of total RNA from the infected cells (top panel) or 1 μL of the culture supernatant (bottom panel). (**$P <$ 0.001 by Student's t test).

gradient and accumulate at the areas with higher $[Ca^{2+}]_c$ (Yi *et al.* 2004).

2BC proteins of the *Picornaviridae* family, with their membrane-targeting properties, are known to play important roles in the alteration of the membranous organelles during virus infections. For example, studies indicated that the hepatitis A virus (HAV) 2BC protein induced intracellular membrane remodeling and permeability (Teterina *et al.* 1997; Jecht *et al.* 1998). The foot-and-mouth disease virus (FMDV) 2BC was reported to perturb the host secretory pathway by blocking the vesicular transport between ER and Golgi (Moffat *et al.* 2005). The poliovirus 2BC was also shown to be a multifunctional protein that participated in the virus-induced membrane proliferation, rearrangement, permeabilization and the alteration of cellular calcium homeostasis (Cho *et al.* 1994; Aldabe and Carrasco 1995; Aldabe *et al.* 1996, 1997). However, similar information on the roles of the EV-A71 2BC protein was lacking until recently when it was reported that EV-A71 2BC triggered autolysosome formation (Lai *et al.* 2017). Our research further revealed an important function of the EV-A71 2BC protein in the rearrangement of mitochondria during EV-A71 infection. The association of the 2BC protein with the mitochondria may also indicate additional potential functions for the 2BC cleavage products 2B and 2C in apoptosis induction, replication center formation and the inhibition of NF-κB activation (Wang *et al.* 2012; Du *et al.* 2015; Cong *et al.* 2016; Li *et al.* 2016).

Perinuclear redistribution of the mitochondria was found in cells infected by different species of viruses, including African swine fever virus (ASFV) (Rojo *et al.* 1998), herpes simplex virus (HSV) (Murata *et al.* 2000), hepatitis B virus (HBV) (Kim *et al.* 2007), rubella virus (RuV)

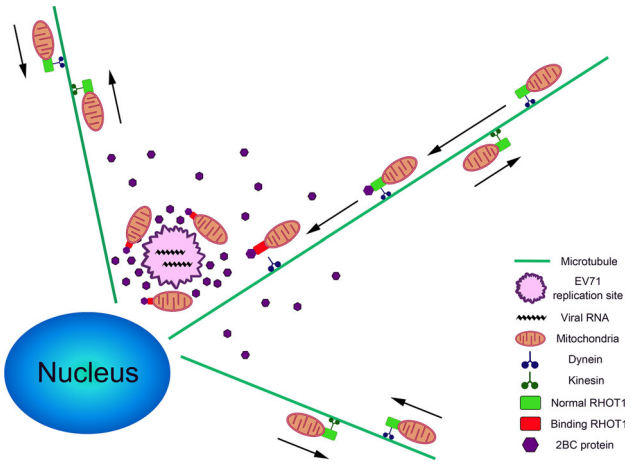

Fig. 7 A model showing the process of mitochondria clustering in the EV-A71-infected cells. Directions of mitochondria movements are indicated with arrows. The legends of different organelles and proteins are shown on the right.

(Beatch *et al.* 2005) and Venezuelan equine encephalitis virus (VEEV) (Keck *et al.* 2017). In poliovirus infected cells, although the viral 2B protein was mainly localized on the membranes of the ER and Golgi, it was also reported to be partially associated with the mitochondria and to induce mitochondria perinuclear clustering (de Jong *et al.* 2008; Madan *et al.* 2008; Martinez-Gil *et al.* 2011). In addition to mitochondria redistribution, all these viruses have also been found to bring about various impacts on mitochondrial activities, including Ca^{2+} uptake (Lund and Ziola 1985; Bouchard *et al.* 2001; Brisac *et al.* 2010; Yang and Bouchard 2012), mitochondrial apoptotic pathway and innate immunity (Belov *et al.* 2003; Shirakata and Koike 2003; Tanaka *et al.* 2004; Autret *et al.* 2007; Ilkow *et al.* 2011; Kim *et al.* 2013; Wang *et al.* 2013; Xiao *et al.* 2013; Claus *et al.* 2015; Cong *et al.* 2016; Kim *et al.* 2017). The mitochondrion is a crucial organelle for the maintenance of cellular homeostasis. The recruitment of the mitochondria to the virus replication sites may facilitate the potential virus-mitochondria interactions and contribute to the viral virulence and pathogenicity. Thus, the mitochondria aggregation process could be a possible target for the development of antivirals. Moreover, perinuclear mitochondria redistribution was also found in fibroblasts from sporadic Alzheimer's disease (sAD) patients and in neuronal cells expressing the cytoplasmic prion protein (CyPrP) (Grenier *et al.* 2006; Wang *et al.* 2008), implying possible relationships between such phenomenon and neurodegenerative disorders. This could provide an inspiration in investigating the pathogenesis of central nervous system (CNS) syndromes in EV-A71-infected patients.

It is thought that the recruitment of mitochondria assisted the replication of viruses mainly by ensuring a sufficient local production of ATP at the virus replication or assembly site. Several researches showed that in ASFV- and RuV-infected cells, the mitochondrial respiratory activity were increased during mitochondria clustering (Rojo *et al.* 1998; Claus *et al.* 2013). Studies also showed that EV-A71 induced the generation of mitochondrial reactive oxygen species (ROS) and a decline in respiratory function, both of which were proven to be essential to EV-A71 replication (Cheng *et al.* 2014). Besides, in most cases, virus infection leads to mitochondria dysfunctions, which seem to contradict with the demand for energy support. Therefore, mitochondria aggregation is more likely to involve in forming an environment that contains structural complexes necessary for virus replication, rather than just to fulfill the energy requirements. When mitochondria are recruited to the perinuclear region, they may become the peripheral part of the virus factories. Subsequently, a series of mitochondrial alterations will take place to accommodate virus replication. It was reported that EV-A71 infection caused an increase in the mitochondrial mass and the abnormal expression of mitochondrial proteins (Cheng *et al.* 2014). The morphological change, alteration of protein expression and even the "dysfunction" of mitochondria are probably accommodations made to optimize the operations of the virus factories and all the mitochondrial proteins and membranes are likely to be materials and tools supporting virus replication in these factories. Our study indicated that the EV-A71 induced mitochondria redistribution was required for virus replication and that microtubule network, dynein motor, calcium signal and the 2BC protein were required for this process. However, the details about the mitochondria-virus interaction and the exact role of mitochondria redistribution in the virus life cycle are still not fully understood. To address these issues, further investigations should focus on the functions of 2BC and changes in the mitochondria after redistribution, such as the expression and activation of mitochondrial proteins and the rearrangement of the mitochondrial membranes.

In conclusion, this study identified a novel function of the EV-A71 nonstructural protein 2BC and provided an insight into the regulation of organelle transport in the EV-A71-infected cells.

Acknowledgements This work was supported by grants from the National Natural Science Foundation of China (NSFC) (Grants Nos. 81621091, 31370201). We are grateful to Prof. Paul Chu, Guest Professor of the Institute of Microbiology, Chinese Academy of Sciences (CAS), for his help during the preparation of the manuscript. We thank Xiaolan Zhang and Tong Zhao, Institute of Microbiology, CAS, for technical help with confocal microscopy and flow cytometry. We also thank Fulian Liao and Weihua Zhuang for their assistance with the experiments.

Author Contributions YY, HC and PT designed the research. YY and HC performed the experiments. ND, XH, LS, WZ and CL

provided experiment support. YY and HC wrote the manuscript. All authors have read and approved the final manuscript for submission.

Compliance with Ethical Standards

Conflict of interest The authors declare that they have no conflict of interest.

Animal and Human Rights Statement This article does not contain any studies with human or animal subjects performed by any of the authors.

References

Aldabe R, Carrasco L (1995) Induction of membrane proliferation by poliovirus proteins 2C and 2BC. Biochem Biophys Res Commun 206:64–76

Aldabe R, Barco A, Carrasco L (1996) Membrane permeabilization by poliovirus proteins 2B and 2BC. J Biol Chem 271:23134–23137

Aldabe R, Irurzun A, Carrasco L (1997) Poliovirus protein 2BC increases cytosolic free calcium concentrations. J Virol 71:6214–6217

Arunagiri C, Macreadie I, Hewish D, Azad A (1997) A C-terminal domain of HIV-1 accessory protein Vpr is involved in penetration, mitochondrial dysfunction and apoptosis of human CD^{4+} lymphocytes. Apoptosis 2:69–76

Autret A, Martin-Latil S, Mousson L, Wirotius A, Petit F, Arnoult D, Colbere-Garapin F, Estaquier J, Blondel B (2007) Poliovirus induces Bax-dependent cell death mediated by c-Jun NH2-terminal kinase. J Virol 81:7504–7516

Beatch MD, Everitt JC, Law LJ, Hobman TC (2005) Interactions between rubella virus capsid and host protein p32 are important for virus replication. J Virol 79:10807–10820

Belov GA, Romanova LI, Tolskaya EA, Kolesnikova MS, Lazebnik YA, Agol VI (2003) The major apoptotic pathway activated and suppressed by poliovirus. J Virol 77:45–56

Bouchard MJ, Wang LH, Schneider RJ (2001) Calcium signaling by HBx protein in hepatitis B virus DNA replication. Science 294:2376–2378

Brisac C, Teoule F, Autret A, Pelletier I, Colbere-Garapin F, Brenner C, Lemaire C, Blondel B (2010) Calcium flux between the endoplasmic reticulum and mitochondrion contributes to poliovirus-induced apoptosis. J Virol 84:12226–12235

Campanella M, de Jong AS, Lanke KW, Melchers WJ, Willems PH, Pinton P, Rizzuto R, van Kuppeveld FJ (2004) The coxsackievirus 2B protein suppresses apoptotic host cell responses by manipulating intracellular Ca^{2+} homeostasis. J Biol Chem 279:18440–18450

Cheng ML, Weng SF, Kuo CH, Ho HY (2014) Enterovirus 71 induces mitochondrial reactive oxygen species generation that is required for efficient replication. PLoS ONE 9:e113234

Cho MW, Teterina N, Egger D, Bienz K, Ehrenfeld E (1994) Membrane rearrangement and vesicle induction by recombinant poliovirus 2C and 2BC in human cells. Virology 202:129–145

Claus C, Schonefeld K, Hubner D, Chey S, Reibetanz U, Liebert UG (2013) Activity increase in respiratory chain complexes by rubella virus with marginal induction of oxidative stress. J Virol 87:8481–8492

Claus C, Manssen L, Hubner D, Rossmark S, Bothe V, Petzold A, Grosse C, Reins M, Mankertz A, Frey TK, Liebert UG (2015) Activation of the mitochondrial apoptotic signaling platform during rubella virus infection. Viruses 7:6108–6126

Cong H, Du N, Tian H, Yang Y, Zhang W, Zhang H, Zhang W, Song L, Tien P (2013) Enterovirus 71 VP1 activates calmodulin-dependent protein kinase II and results in the rearrangement of vimentin in human astrocyte cells. PLoS ONE 8:e73900

Cong H, Du N, Yang Y, Song L, Zhang W, Tien P (2016) Enterovirus 71 2B induces cell apoptosis by directly inducing the conformational activation of the proapoptotic protein bax. J Virol 90:9862–9877

Danishuddin M, Khan SN, Khan AU (2010) Molecular interactions between mitochondrial membrane proteins and the C-terminal domain of PB1-F2: an in silico approach. J Mol Model 16:535–541

de Jong AS, Visch HJ, de Mattia F, van Dommelen MM, Swarts HG, Luyten T, Callewaert G, Melchers WJ, Willems PH, van Kuppeveld FJ (2006) The coxsackievirus 2B protein increases efflux of ions from the endoplasmic reticulum and Golgi, thereby inhibiting protein trafficking through the Golgi. J Biol Chem 281:14144–14150

de Jong AS, de Mattia F, Van Dommelen MM, Lanke K, Melchers WJ, Willems PH, van Kuppeveld FJ (2008) Functional analysis of picornavirus 2B proteins: effects on calcium homeostasis and intracellular protein trafficking. J Virol 82:3782–3790

Dixit R, Ross JL, Goldman YE, Holzbaur EL (2008) Differential regulation of dynein and kinesin motor proteins by tau. Science 319:1086–1089

Du H, Yin P, Yang X, Zhang L, Jin Q, Zhu G (2015) Enterovirus 71 2C Protein Inhibits NF-kappaB Activation by Binding to RelA (p65). Sci Rep 5:14302

Gogvadze V, Orrenius S (2006) Mitochondrial regulation of apoptotic cell death. Chem Biol Interact 163:4–14

Grenier C, Bissonnette C, Volkov L, Roucou X (2006) Molecular morphology and toxicity of cytoplasmic prion protein aggregates in neuronal and non-neuronal cells. J Neurochem 97:1456–1466

Hollenbeck PJ, Saxton WM (2005) The axonal transport of mitochondria. J Cell Sci 118:5411–5419

Huang CC, Liu CC, Chang YC, Chen CY, Wang ST, Yeh TF (1999) Neurologic complications in children with enterovirus 71 infection. N Engl J Med 341:936–942

Ilkow CS, Goping IS, Hobman TC (2011) The Rubella virus capsid is an anti-apoptotic protein that attenuates the pore-forming ability of Bax. PLoS Pathog 7:e1001291

Jecht M, Probst C, Gauss-Muller V (1998) Membrane permeability induced by hepatitis A virus proteins 2B and 2BC and proteolytic processing of HAV 2BC. Virology 252:218–227

Keck F, Brooks-Faulconer T, Lark T, Ravishankar P, Bailey C, Salvador-Morales C, Narayanan A (2017) Altered mitochondrial dynamics as a consequence of Venezuelan Equine encephalitis virus infection. Virulence. https://doi.org/10.1080/21505594.2016.1276690:1-18

Kim S, Kim HY, Lee S, Kim SW, Sohn S, Kim K, Cho H (2007) Hepatitis B virus x protein induces perinuclear mitochondrial clustering in microtubule- and Dynein-dependent manners. J Virol 81:1714–1726

Kim SJ, Khan M, Quan J, Till A, Subramani S, Siddiqui A (2013) Hepatitis B virus disrupts mitochondrial dynamics: induces fission and mitophagy to attenuate apoptosis. PLoS Pathog 9:e1003722

Kim JA, Kim JC, Min JS, Kang I, Oh J, Ahn JK (2017) HSV-1 ICP27 induces apoptosis by promoting Bax translocation to mitochondria through interacting with 14-3-3theta. BMB Rep 50:257–262

Lai JKF, Sam IC, Verlhac P, Baguet J, Eskelinen EL, Faure M, Chan YF (2017) 2BC non-structural protein of enterovirus A71 interacts with SNARE proteins to trigger autolysosome formation. Viruses 9:169

Li Q, Zheng Z, Liu Y, Zhang Z, Liu Q, Meng J, Ke X, Hu Q, Wang H (2016) 2C proteins of enteroviruses suppress IKKbeta phosphorylation by recruiting protein phosphatase 1. J Virol 90:5141–5151

Liu X, Hajnoczky G (2009) Ca^{2+}-dependent regulation of mitochondrial dynamics by the Miro-Milton complex. Int J Biochem Cell Biol 41:1972–1976

Lund K, Ziola B (1985) Cell sonicates used in the analysis of how measles and herpes simplex type 1 virus infections influence Vero cell mitochondrial calcium uptake. Can J Biochem Cell Biol 63:1194–1197

Madan V, Castello A, Carrasco L (2008) Viroporins from RNA viruses induce caspase-dependent apoptosis. Cell Microbiol 10:437–451

Martinez-Gil L, Bano-Polo M, Redondo N, Sanchez-Martinez S, Nieva JL, Carrasco L, Mingarro I (2011) Membrane integration of poliovirus 2B viroporin. J Virol 85:11315–11324

McBride HM, Neuspiel M, Wasiak S (2006) Mitochondria: more than just a powerhouse. Curr Biol 16:R551–R560

Moffat K, Howell G, Knox C, Belsham GJ, Monaghan P, Ryan MD, Wileman T (2005) Effects of foot-and-mouth disease virus nonstructural proteins on the structure and function of the early secretory pathway: 2BC but not 3A blocks endoplasmic reticulum-to-Golgi transport. J Virol 79:4382–4395

Murata T, Goshima F, Daikoku T, Inagaki-Ohara K, Takakuwa H, Kato K, Nishiyama Y (2000) Mitochondrial distribution and function in herpes simplex virus-infected cells. J Gen Virol 81:401–406

Rojo G, Chamorro M, Salas ML, Vinuela E, Cuezva JM, Salas J (1998) Migration of mitochondria to viral assembly sites in African swine fever virus-infected cells. J Virol 72:7583–7588

Schmidt NJ, Lennette EH, Ho HH (1974) An apparently new enterovirus isolated from patients with disease of the central nervous system. J Infect Dis 129:304–309

Seth RB, Sun L, Chen ZJ (2006) Antiviral innate immunity pathways. Cell Res 16:141–147

Shirakata Y, Koike K (2003) Hepatitis B virus X protein induces cell death by causing loss of mitochondrial membrane potential. J Biol Chem 278:22071–22078

Solomon T, Lewthwaite P, Perera D, Cardosa MJ, McMinn P, Ooi MH (2010) Virology, epidemiology, pathogenesis, and control of enterovirus 71. Lancet Infect Dis 10:778–790

Tanaka Y, Kanai F, Kawakami T, Tateishi K, Ijichi H, Kawabe T, Arakawa Y, Kawakami T, Nishimura T, Shirakata Y, Koike K, Omata M (2004) Interaction of the hepatitis B virus X protein (HBx) with heat shock protein 60 enhances HBx-mediated apoptosis. Biochem Biophys Res Commun 318:461–469

Tang F, Xia H, Wang P, Yang J, Zhao T, Zhang Q, Hu Y, Zhou X (2014) The identification and characterization of nucleic acid chaperone activity of human enterovirus 71 nonstructural protein 3AB. Virology 464:353–364

Teterina NL, Bienz K, Egger D, Gorbalenya AE, Ehrenfeld E (1997) Induction of intracellular membrane rearrangements by HAV proteins 2C and 2BC. Virology 237:66–77

van Kuppeveld FJ, Hoenderop JG, Smeets RL, Willems PH, Dijkman HB, Galama JM, Melchers WJ (1997) Coxsackievirus protein 2B modifies endoplasmic reticulum membrane and plasma membrane permeability and facilitates virus release. EMBO J 16:3519–3532

Wang T, Weinman SA (2013) Interactions between hepatitis C virus and mitochondria: impact on pathogenesis and innate immunity. Curr Pathobiol Rep 1:179–187

Wang X, Su B, Fujioka H, Zhu X (2008) Dynamin-like protein 1 reduction underlies mitochondrial morphology and distribution abnormalities in fibroblasts from sporadic Alzheimer's disease patients. Am J Pathol 173:470–482

Wang J, Wu Z, Jin Q (2012) COPI is required for enterovirus 71 replication. PLoS ONE 7:e38035

Wang B, Xi X, Lei X, Zhang X, Cui S, Wang J, Jin Q, Zhao Z (2013) Enterovirus 71 protease 2Apro targets MAVS to inhibit anti-viral type I interferon responses. PLoS Pathog 9:e1003231

Weidman MK, Sharma R, Raychaudhuri S, Kundu P, Tsai W, Dasgupta A (2003) The interaction of cytoplasmic RNA viruses with the nucleus. Virus Res 95:75–85

Xiao CX, Yang XN, Huang QW, Zhang YQ, Lin BY, Liu JJ, Liu YP, Jazag A, Guleng B, Ren JL (2013) ECHS1 acts as a novel HBsAg-binding protein enhancing apoptosis through the mitochondrial pathway in HepG2 cells. Cancer Lett 330:67–73

Yang B, Bouchard MJ (2012) The hepatitis B virus X protein elevates cytosolic calcium signals by modulating mitochondrial calcium uptake. J Virol 86:313–327

Yi M, Weaver D, Hajnoczky G (2004) Control of mitochondrial motility and distribution by the calcium signal: a homeostatic circuit. J Cell Biol 167:661–672

Yi EJ, Shin YJ, Kim JH, Kim TG, Chang SY (2017) Enterovirus 71 infection and vaccines. Clin Exp Vaccine Res 6:4–14